From waste to value

Anagnostopoulos, Argyrios; Elena Navarro, M.; Sharma, Shivangi; Ahmad, Abdalqader; Maksum, Yelaman; Ding, Yulong

DOI:
10.1016/j.solener.2023.112294

Solar Energy 268 (2024) 112294

Contents lists available at ScienceDirect

Solar Energy

journal homepage: www.elsevier.com/locate/solener

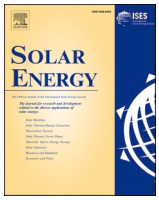

From waste to value: Utilising waste foundry sand in thermal energy storage as a matrix material in composites

Argyrios Anagnostopoulos [a,b,c,*], M. Elena Navarro [a,*], Shivangi Sharma [a], Abdalqader Ahmad [a], Yelaman Maksum [a], Yulong Ding [a]

[a] Dr Argyrios Anagnostopoulos, Dr Maria Elena Navarro, Dr Shivangi Sharma, Dr Abdalqader Ahmad, Yelaman Maskum, Prof. Yulong Ding, Birmingham Centre for Energy Storage & School of Chemical Engineering, University of Birmingham, Birmingham B15 2TT, United Kingdom
[b] Department of Mechanical Engineering, Aristotle University of Thessaloniki, PO Box 454, 54124, Thessaloniki, Greece
[c] Institute of Chemistry, University of Silesia, 40-006 Katowice, Poland

ARTICLE INFO

Keywords:
Foundry sand
Composite
Phase change
Latent heat storage
Waste heat recovery
Upcycling

ABSTRACT

Waste foundry sand (WFS) is a by-product of the casting industry, which poses increasing economic and environmental issues due to the costs associated with landfill maintenance and stricter environmental regulations. This study proposes a novel solution for WFS as a material for thermal energy storage. The approach involves blending WFS with $NaNO_3$ and a proprietary additive, X, to fabricate a composite phase change material (CPCM). The CPCM is found to be structurally stable up to 400 °C, and an optimal composition with a mass ratio of $NaNO_3$:WFS:X = 0.6:0.3:0.1 is achieved. This composition yields an energy storage density of 628 ± 27 kJ/kg, and an average thermal conductivity of 1.38 W/mK over the temperature range of 25–400 °C. The CPCM also exhibits good mechanical strength and a low coefficient of thermal expansion compared to $NaNO_3$. Currently, only a small portion of WFS is recycled, most commonly in building applications. The CPCM presented in this study has the potential for medium-to-high temperature heat storage in waste heat recovery applications, offering a sustainable solution for upcycling WFS.

1. Introduction

The foundation industries underpin many aspects of our economy but are also among the most challenging sectors to decarbonise in a sustainable manner [12]. The EU has set an ambitious target of a 42 % reduction in industrial sector carbon by 2030 [13]. According to a European Union assessment, industries are responsible for 27 % of the total energy uptake and contribute to 30 % of the CO2 emissions linked to heating [21]. Thermal procedures represent 70 % of the energy requirement within the industry, translating to 18.9 % of the collective energy consumption across the EU [35]. Thermal processes emit a large amount of waste heat with almost one-fifth (~400 TWh/yr) being classified as high-grade, hence with good potential for recovery and reuse [2].

Consequently, waste heat recovery (WHR) emerges as pivotal for sectors with high energy consumption such as the industrial sector [24]. Among the available WHR technologies, thermal energy storage (TES) has the potential to solve the discontinuous waste heat supply and heat demand mismatch problem [37]. TES can thus overcome the issue of temporal and geographical mismatch faced by technologies such as recuperators, regenerators and heat pipes. Its flexible design adjusts process components to lower maximum output, avoiding start-up and partial load losses [37]. This reduces capital investment compared to other WHR technologies, such as thermoelectric generators or Organic Rankine Cycle engines, making it a cost-effective solution to energy efficiency problems [14].

TES is broadly classified into sensible, latent, and thermochemical; the third is still at a material stage in medium–high temperature settings [41]. Sensible TES (STES) is a mature technology that uses inexpensive materials and has been applied on a large scale for hundreds of years but it exhibits low energy density and quick temperature drops during discharge [41]. Latent heat TES (LHTES) is based on the capability of a substance, commonly known as the phase change material (PCM), to absorb or dispel heat at a consistent temperature during its phase transition. It has been extensively investigated in recent years, and large-scale industrial deployments have been reported for peak electricity grids, solar energy utilisation, and waste heat recovery [25]. It displays minor temperature fluctuation during charging/discharging and has a

* Corresponding authors.
E-mail addresses: a.anagnostopoulos@bham.ac.uk (A. Anagnostopoulos), h.navarro@bham.ac.uk (M. Elena Navarro).

https://doi.org/10.1016/j.solener.2023.112294
Received 4 September 2023; Received in revised form 9 December 2023; Accepted 22 December 2023
Available online 28 December 2023

higher energy density than STES [25]. However, PCMs are not without challenges, including issues like low thermal conductivity, volume expansion, subcooling and corrosion [22]. These drawbacks impact the efficiency of LHTES from the actual devices as well as to broader system operations. Nevertheless, many of these concerns can be mitigated by embedding the PCMs within a porous framework, generally made up of refractory materials [5,6]. The resulting materials are called composite phase change materials (CPCMs). CPCMs, aside from LHTES, can also be effectively applied in combined STES-LHTES systems. Such hybrid TES systems have been shown to be extremely promising alternatives [1]. Currently, only part of the WFS is utilised primarily on geotechnical applications, such as road embankments and bases, or as an additive in concrete.

Waste foundry sand (WFS) is a by-product/waste from metal casting processes in the ferrous and non-ferrous metal casting industries. In a typical casting process, fresh sand is used to construct moulds in which the metal is poured in the desired shape. After solidification, the metal is extracted, and the sand is reused. Several approaches have been followed to recycle the sand internally in the foundries, reaching an average internal recycling rate of up to 80–98 %. However, this recycled sand can only be used for a finite number of casting cycles until quality standards are not met, at which point fresh sand is introduced into the mould. This massive surplus of sand is disposed of in landfills as metal casting necessitates large volumes of sand that cannot be accommodated in foundry warehouses [47]. WFS disposal is expensive due to increased transportation costs and high landfill taxes [36]. A 2020 survey by the Cast Metal Federation (CMF, UK) found that it accounts for 4 % of the annual turnover of an average sand foundry. China, India, and the USA are the world's largest producers of WFS, with a combined total of roughly 71 million tonnes[45]. A small fraction of WFS has applications in concrete production, low-strength controlled materials, and road pavement materials [18]. Other novel proposed strategies include its use as a ground barrier against wet leakage from landfill sites and as a structural constituent in organic waste. However, the utilisation rate of WFS is still low [48].

The chemical composition of WFS (ceramic), density, particle size ($0.15\ mm < D < 0.6\ mm$), and specific surface area make it a fairly good candidate as a supporting material for a CPCM [48]. This work focuses on CPCM for the medium-to-high-temperature range (>200 ℃). Streams at these temperatures are commonly present in foundation industries [42]. This provides a novel utilisation pathway for recycling the WFS as a key material for CPCMs for capturing, storing, and reusing waste heat.

2. Materials and methods

2.1. Materials

The PCM material used in this work is $NaNO_3$. It is purchased from Sigma-Aldrich at chemical grade purity (>99.9 %). A proprietary additive, X, was used to improve the structural stability of the CPCM. Such an additive was identified by Birmingham Centre for Enegry Storage, which contains only natural materials including clay and is fully recyclable at their end of life. Specifically, this additive is Bentonite in sodium form purchased from Thermo Fisher Scientific with > 99 % purity.

The matrix material of the CPCM was the waste foundry sand obtained from "Boro Foundry", a West Midlands (UK) based specialist manufacturer-supplier of a wide range of castings and machine parts using a variety of ferrous and non-ferrous metals. The chemical composition of the sand can be seen in Table 1. WFS exhibits a composition with SiO_2 being its predominant component at 87.91 %, followed by Al_2O_3 at 4.7 % and Fe_2O_3 at 0.94 %. What is notable is that unlike sand, the content of silica in WFS is somewhat lower. It should be noted that the physical and chemical properties can differ based on its source, casting method, additives, recycling frequency, and binders used [9]. With regards to the particle shape WFS varies from sub-angular to round [26].

2.2. Fabrication of composite phase change materials

The fabrication of the CPCMs involves a comminution process, which utilises a mortar and pestle for homogenisation, followed by hand-stirring. Subsequently, the mixture is shaped into 13 mm pellets under a constant pressure of 60 MPa for 2 min using a press. The pellets are then sintered at 400 °C with a heating rate of 5 °C/min in a high-temperature ceramic furnace (HTF 18/27, Carbolite, UK). After sintering, the pellets are cooled to room temperature to acquire a shape-stable structure, which undergoes characterisation analysis.

A preliminary investigation was conducted to evaluate the viability of various compositions of WFS-salt CPCMs. The main objective of CPCM design is to enhance thermal performance by increasing PCM content and minimising porosity. However, poor cohesion of the sand in WFS-salt CPCMs caused instability even at a 70–30 (WFS-salt) mass ratio. This is due to the uniform grain size distribution of WFS, with about 85–95 % of its composition lying between 0.6 mm and 0.15 mm sieve sizes. This uniformity, coupled with its sub-angular to round particle shape, likely contributes to poorer cohesion, causing instability [40].

To improve stability, an additive, X, was introduced. X plays a pivotal role in enhancing the structural stability of the CPCM. It acts as a binder by improving particle adhesion, leading to a more cohesive and stable structure. This is achieved through its thixotropic properties, which allow it to form a gel-like matrix when mixed with water, enhancing the binding between the WFS particles. This results in a CPCM that is more resistant to the stresses induced during the phase change process, especially considering the large volume changes and the higher CTE of the PCM compared to WFS. X's use in this context builds upon applications in thermochemical energy storage composites as well as in low-temperature CPCMs for building applications [3,50]. A series of four compositions are evaluated, and in each case, the additive and the salt were first milled and mixed, and water was then added. Water could create holes due to bubbling, but this was avoided by maintaining the CPCMs at 80 °C for 3 h to slowly evaporate any water before reaching its boiling point. The resulting pellets were then heat-treated as described above. The water content (%) is calculated as a fraction of the additive mass. Table 2 summarises the four compositions evaluated in this study.

After sintering, Sample 4 exhibited complete failure, with noticeable structural degradation and salt leakage (Fig. 1). In Sample 2, PCM leakage is observed, as evidenced by a white ring at the bottom of the pellet, which is confirmed to be solidified salt. Samples 1 and 3, on the

Table 2
Compositions, in wt.%, of WFS-$NaNO_3$-X CPMCs.

Material	Sample 1	Sample 2	Sample 3	Sample 4
$NaNO_3$	55	50	60	60
WFS	30	45	30	35
X (additive)	15	5	10	5
Water	0.029	0.014	0.029	0.014

Table 1
Compositions, in wt.%, of WFS [28].

Constituent	Ignition loss	SiO_2	Al_2O_3	$Fe2O_3$	CaO	MgO	SO_3	K_2O	Na_2O
WFS	5.15	87.91	4.70	0.94	0.14	0.30	0.09	0.25	0.19

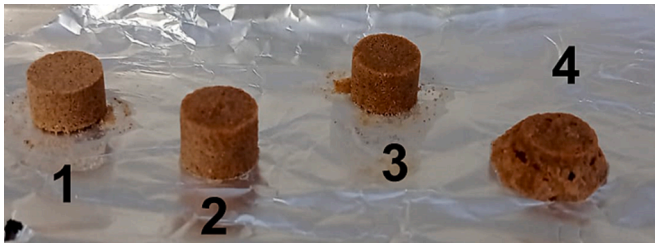

Fig. 1. Preliminary samples (left to right) prepared after heat treatment.

other hand, are found to be structurally stable. To further ensure accuracy, two additional samples for each of the stable compositions were prepared for testing. These samples are subsequently subjected to thermal cycling followed by characterisation.

2.3. Methods

The sand's grain density is determined using a helium-based pycnometer (Accupyc II 1340, Micromeritics), yielding a value of 2.51 ± 0.06 g/cm^3. To measure the bulk density of the developed CPCMs, the mass and volume (dimensions) of individual pellets is guaged. Subsequently, the porosity of the CPCM is deduced from the density ratio.

The latent heat, melting point and specific heat capacity of the samples fabricated in this work is determined through Differential Scanning Calorimetry (DSC). These assessments are conducted using a DSC3 Mettler Toledo instrument, ranging from 20 to 400 °C at a ramping speed of 10 °C per minute. The samples are first placed in aluminum crucibles. The tests are performed in an ambient air environment with a gas flow rate of air at 100 ml/min. For specific heat determinations, we adhere to DIN51007 guidelines and employ the sapphire method [39].

The Laser Flash Technique (LFA) using an LFA 427 apparatus (Netzsch) is chosen to measure both thermal conductivity and diffusivity. To ensure optimal readings, the sample surfaces are always ensured to be level and are then subsequently spray coated with graphite through a controlled protocol. This coating is essential as it mitigates direct laser interaction and facilitates efficient energy transfer within the sample. Tests are executed with an airflow setting of 100 ml/min. Based on these readings, the thermal conductivity is calculated using the below formula:

$$\lambda = a(T)\rho(\mathrm{T})C_p(T) \tag{1}$$

where, T is temperature (K), α is thermal diffusivity (mm^2/s), ρ is density (g/cm^3) and C_p is heat capacity (J/gK).

Thermogravimetric analysis is conducted using simultaneous differential/thermogravimetric scanning instruments (STA 449F3, Netzch). Samples, weighing approximately 10 mg each, are placed in a platinum crucible. The analysis spans a temperature range of 25 to 500 °C at a steady heating rate of 10 °C/min, all under ambient air conditions.

For insights into microstructure and pore size distribution, X-ray nano-CT Skyscan 2211 is employed. Analyzed samples are cylindrical, measuring φ 2 × 15 mm. During the X-ray tomography tests, a voltage of 95 kV and a current of 150 μA are maintained. Projection images are captured at 0.1° intervals throughout a complete 180° rotation, offering a pixel resolution of 9.5 μm. Following the scans, the Recon software is used to produce a data file that furnishes three-dimensional details for each specimen. The reconstructed 3D data sets are subsequently analyzed and visualized using the CTan software.

Using an optical dilatometer, DILA-806 (TA instrument), the coefficient of thermal expansion is ascertained. This process involves heating cylindrical samples, roughly 13 mm in diameter, from ambient temperature to 500℃ at a rate of 5 K/min, all in an air environment. Compressive strength evaluations are facilitated by a universal mechanical testing apparatus (LS100, Lloyd Instruments CO., LTD., UK). Load is applied on the samples, in a sustained manner, until they reach the point of rupture. Based on the data generated during the test, the elastic modulus is subsequently derived through the following formula:

$$E = \frac{\Delta H}{H}\Delta\sigma \tag{2}$$

where, E is the elastic modulus (MPa), H the sample height (m), ΔH the change in sample height from the start of compression until breakage (g/cm^3) and $\Delta\sigma$ the compressive strength (MPa).

The protocol followd for thermal cycling involved increasing the temperature to 400 °C, maintaining it at this level for thirty minutes, then reducing it to 270 °C, where it was held for an additional ten minutes. This procedure was repeated for a total of 48 cycles. Such initial findings shed light on the structural resilience and thermal efficacy of the WFS-salt CPCMs when subjected to designated cycling scenarios and for different material formulations.

3. Results and discussion

CPCMs selected in the screening tests perform well after thermal cycling. Their structure appears to be largely intact with minor deformations due to the granular structure of the WFS (Fig. 2). Among the CPCMs tested, Na55 (Sample 1) stands out with significantly smaller pores and a lower number of defects compared to Na60 (Sample 3).

This is in line with the density and porosity measurements, which show that Na60 has a higher density (8.8 %) and lower porosity (21.3 %) due to its higher X content. This is surprising, as one would expect a lower liquid content to translate to increased CPCM stability. However, an increased amount of X translates to a higher percentage of water in the CPCM. In fact, the pores on the CPCM surface appear to have spherical shapes resembling water evaporation sites. The second reason for the higher porosity of Na60 is the swelling properties of X [46]. Swelling is known to be detrimental to the structural stability of CPCMs [15].

Looking at the sample images in Fig. 2 numerous pores within the CPCM's structure are evident. However, the average measured porosity level is approximately 28 %, which is consistent with the expected range for densely packed granular materials, where theoretical packing density allows for a minimum of 26 % void space. This porosity is instrumental in accommodating the thermal expansion of sodium nitrate ($NaNO_3$), which exhibits a volume change of around 9.7 % during its phase transition, and a thermal expansion mismatch of approximately 3 % with the matrix material. The sum of these changes results in an estimated 12.7 % volume increase during heating and phase transition. If the porosity were significantly lower, then this collective expansion could lead to stress on the matrix due to confined pressurization, raising the potential for leakage or structural collapse. Therefore, the observed porosity in Na60 not only contributes to the material's thermal function by allowing space for the PCM expansion but also plays a critical role in maintaining structural integrity during the phase change.

With respect to thermal evolution, density appears to increase and porosity to decrease with further cycling. This indicates that the structure is most likely physically stable, but there is some degree of mass loss. The mass loss is related to the chemical stability of X. In fact, throughout the temperature range between 150 and 600 °C, Na-X demonstrates chemical degradation due to the loss of structural hydroxyl groups [27]. Nevertheless, the density and porosity of both samples appear to stabilise after 48 cycles, which denotes that almost the entirety of X's thermal decomposition is realised and the CPCM physical stability is still maintained.

To further establish the chemical stability of the CPCM, a thermogravimetric analysis (TGA) was performed on the cycled samples (Fig. 3). The TGA curves are the average behavior of three independent samples for Na55 and Na60 respectively. They illustrate the mass change over time alongside the temperature profile of the samples as they are heated.

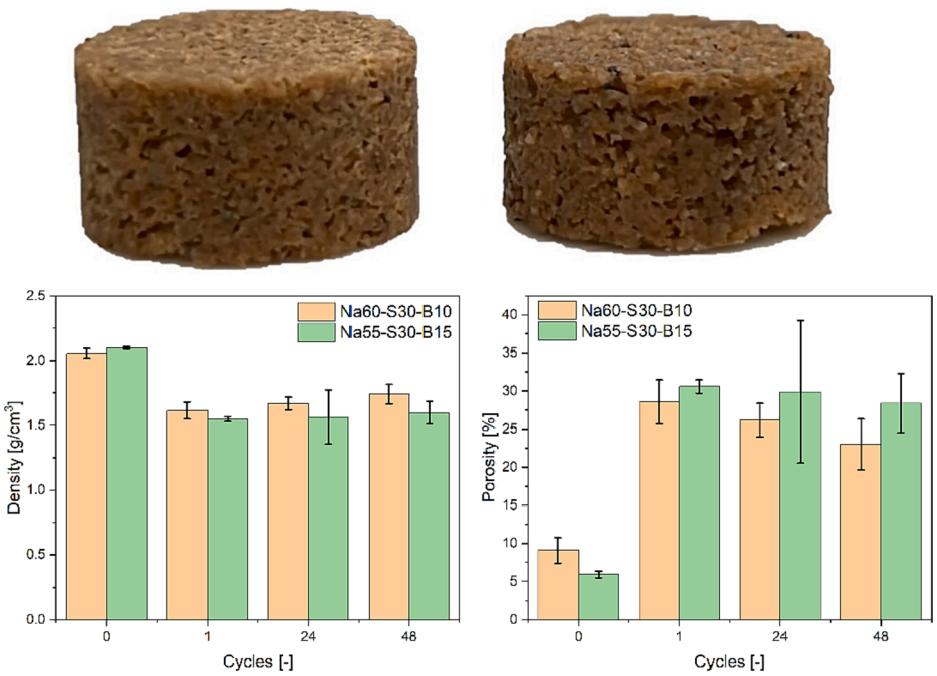

Fig. 2. Top: Sample 1 (left) and Sample 3 (right) CPCMs after thermal cycling. Bottom: Density (left) and porosity (right) evolution of the fabricated CPCMs during thermal cycling.

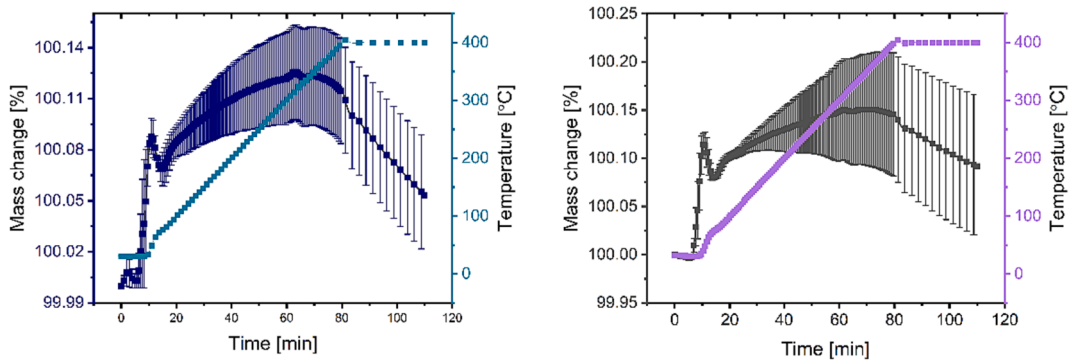

Fig. 3. Thermogravimetric analysis (TGA) of CPCM samples Na55 (left) and Na60 (right), showing the mass change percentage over time and corresponding temperature profiles.

In both samples, the mass remains relatively stable up to around 400 °C, with no significant signs of mass loss, which implies that no degradation of the proprietary additive X, or other volatile components within the CPCM occurs until the temperature threshold is reached.

For Samples Na55 and Na60, the TGA curves show minimal fluctuations, which could be attributed to the absorption of atmospheric gases or instrumental sensitivity. However, this slight deviation is well within the error margin of the TGA equipment and sample variability. Such minor variations are expected in high-precision thermal analyses and do not indicate any considerable material loss or degradation.

These findings are indicative of a material composition that is well-suited for TES-WHR applications in the proposed operational temperature range without degradation or compromise to its structural integrity.

Regarding the structural performance of the materials, the results of the SEM analysis suggest that the difference between Na55 and Na60 can be attributed to the inhomogeneity of their X and WFS content (Fig. 4). The microstructure of Na55 appears to be coarser, with several large, valley-like pores and a clear separation between the X, salt, and WFS (white filler sand) components. The large smooth areas correspond to the X, while the white grit-textured chunks and regions correspond to the salt and WFS, respectively. The X appears to be poorly mixed with the other components and is agglomerated in big areas

On the other hand, the microstructure of Na60 appears to be denser, with fewer large millimetre pores and a well-mixed composition. All three components, X, salt, and WFS, are well blended, and the X structure is almost indistinguishable from the sand. This coupled with the salt's wetting and adherence to the silica-based WFS is pivotal for preventing the PCM from leaking during the phase change. In fact this favorable wetting contact angle and the high surface tension allows the molten salt to spread across and adhere to the WFS, promoting a stable matrix and minimizing leakage risks.

Regarding the visible microstructural differences these are likely due to the higher percentage of X in Na55 compared to Na60. Although the higher X content improves the structural stability of the CPCM, an excess of X can lead to an imbalance in the proportion of X, salt, and WFS. This results in an inhomogeneous mixture, evident in the SEM images of Na55.The comparative analysis highlights that beyond the quantity of X, it is the distribution that is integral to the structural stability and the prevention of leakage in CPCMs. While Na55′s higher X content does fortify the structural framework, it also resulted in a non-uniform distribution. Na60, with its more unirform composition, illustrates how a balanced ratio and even distribution of components are critical to the

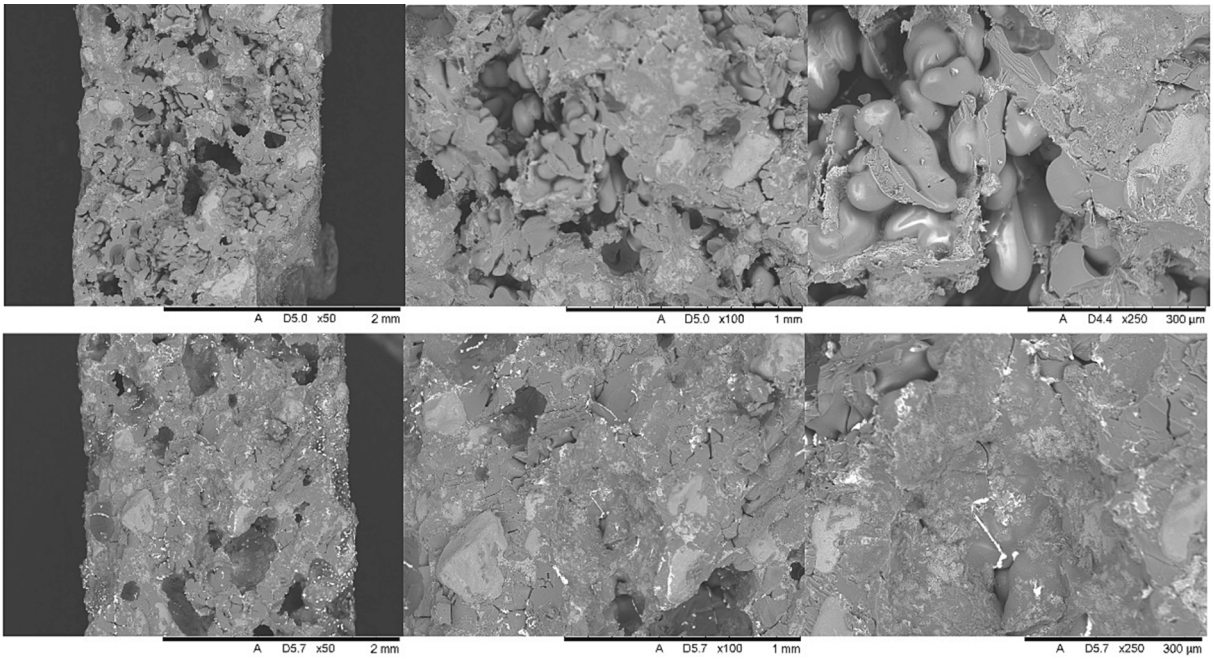

Fig. 4. Scanning electron microscopy snapshots at (left to right) x50, x100 and x250 of Top: Na55 and Bottom: Na60.

structural integrity of the CPCM.

Overall, these results suggest that the composition of the CPCM plays a crucial role in its structural stability and performance. A well-balanced mixture of X, salt, and WFS is essential for maintaining the integrity of the CPCM during thermal cycling. Further research may be necessary to determine the optimal ratios of these components for improving the performance of CPCMs.

With respect to PCM fraction, the CPCMs perform reasonably. PCM fraction is the bottleneck in the CPCM design. Most studies involving $NaNO_3$ as a PCM typically report fractions of up to 60 %. Higher fractions result in instability due to PCM leakage, structural collapse, or a combination of both. X can thus play a key role in enabling the use of more matrix materials that would otherwise result in unstable composites. In fact, Guo and Wang prepared CPCMs consisting of SiO_2 as a matrix material and $NaNO_3$ and found that the CPCM was leaking during heating above 60 % $NaNO_3$ content [19]. Similar PCM contents are reported by Liu et al. in MgO-$NaNO_3$ CPCMs, even after the addition of water to improve microstructure formation [33]. Yang et al. attempted to valorise stone-sawing mud as a matrix material in a CPCM combined with $NaNO_3$ and found the maximum PCM content to be only 50 % [53].

In previous works involving red mud, a waste from the aluminimum industry, mainly consisting of SiO_2 and Fe_2O_3, we also established similar conclusions with a $NaNO_3$ content higher than 60 % resulting in structural instability/leakage [6].

The DSC results provide insight into the thermal transition characteristics of the CPCM samples (Fig. 5). Notably, the melting point of Na55 (306.6 ± 0.4 °C) appears to be marginally lower than that of Na60 (307.2 ± 0.6 °C), and both deviate slightly from the melting point of pure sodium nitrate, which is 308 °C.

The reduced melting point observed in Na55 could be the result of a more heterogeneous composition within the sample. Such inhomogeneity can lead to a decrease in the crystalline structure's uniformity, facilitating phase change at a reduced temperature [8]. The heterogeneity, in effect, may act to lower the energy barrier necessary for the transition, resulting in the earlier onset of melting as evidenced in the DSC curve.

With respect to latent heat Na60 records a higher experimental latent heat value of 102 J/g compared to 89 J/g for Na55, which is in line with the expected influence of PCM content, given that sodium nitrate has a latent heat of 173 J/g [34]. The marginally lower latent heat of Na55

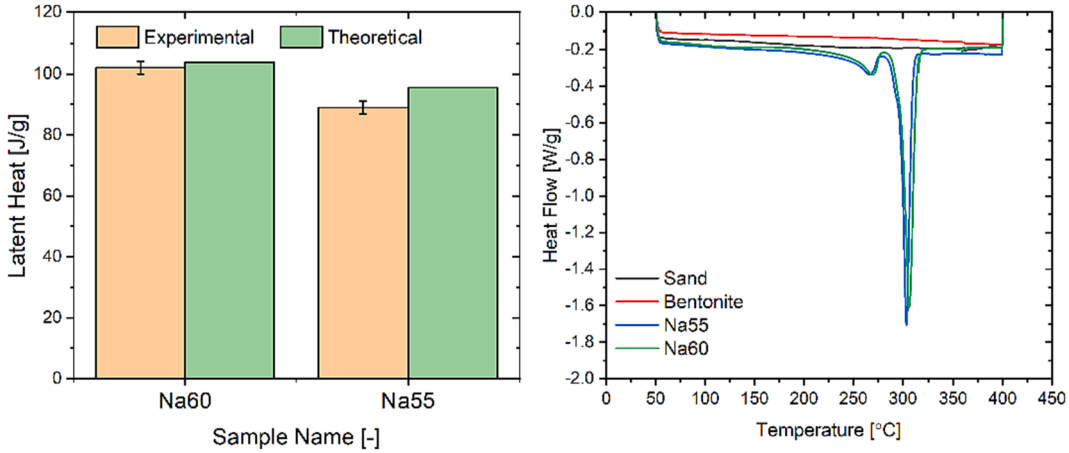

Fig. 5. Experimental and theoretical latent heat values for CPCM samples Na60 and Na55 (left), and DSC curves indicating melting transitions (right).

compared to its theoretical prediction suggests some degree of leakage during thermal cycling or enthalpy reduction, possibly due to PCM confinement as supported by previous research. Such remarks have been made by Mitran in the case of a salt-SiO_2 CPCM and by Xu et al., who observed an average 4.9 % decrease in the latent heat of $NaNO_3$-diatomite CPCM [38,51].

The specific heat capacity (C_p) of the CPCM is a critical factor that governs their efficacy in TES applications. In this work, the Cp is evaluated over a temperature spectrum of 50–400 °C, as depicted in Fig. 6. Sodium nitrate boasts a superior C_p compared to both sand and X. In terms of the CPCM combinations, the peak C_p is noted at 60 wt.% PCM content, displaying an average metric of 1.36 J/gK in its solid state and 1.46 J/gK when liquid. It's crucial to highlight that the derived values for the C_p of the CPCM align with conventional mixing theories pertaining to the C_p of mixtures, given the inherent relative uncertainties of the measurements. Observing the progression of the C_p across temperature, a surge is seen until 250 °C, marked by a noticeable peak near the phase transition points. This spike is more evident in the CPCM specimens and is subdued in WFS. Post this phase shift, the C_p metrics tend to stabilize till 400 ℃. An important consideration is the steps taken to mitigate the DSC's substantial margin of error; samples are positioned in crucibles as pellets of 5 mm diameter. These pellets, which were fabricated with a uniform mass and compression akin to the larger CPCMs, undergo identical cycles to the more sizable samples, which are then subjected to structural/thermal charachterization.

The energy storage density of the proposed CPCM is also calculated using the specific heat capacity latent heat and density data provided in previous sections, in the temperature range of 25–400 °C. As expected, Na60 has a higher energy density (628 ± 27 kJ/kg) compared to Na55 (567 ± 43 kJ/kg) due to its higher density and specific heat capacity. This is higher than a state-of-the-art study on $NaNO_3$/stone-sawing-mud CPCMs, which was found to be up to 444.86 kJ/kg [53]. The energy storage density reported here is higher than sodium nitrate-diatomite CPCMs at similar mass ratios, which was 560 kJ/kg [51].

Thermal conductivity is a critical parameter in CPCM design and significantly impacts a TES system's charging and discharging efficiency based on CPCMs. It governs the power capacity of the TES system and is influenced by various factors.

In the case of WFS pellets, high porosity is expected due to their uniform particle size distribution, which leads to a lower effective thermal conductivity. The thermal conductivity values between Na60-S30-B10 and Na55-S30-B15 increase further as CPCMs with higher PCM content have higher density and specific heat capacity (Fig. 7). The maximum average thermal conductivity is attained in the case of Na60, which is 1.38 W/mK, considerably higher than pure $NaNO_3$ (0.53 W/mK [4].

Several studies have reported the thermal conductivity of different types of CPCMs. Li et al. reported a thermal conductivity of 0.7 W/mK for a $NaNO_3$-expanded vermiculite CPCM [30], while another study found the thermal conductivity of a $NaNO_3$-expanded perlite CPCM at a 60–40 mass ratio to be 0.57 W/mK [31]. In the case of NaNO3-iron tailings CPCMs at 50–50 mass ratio, the thermal conductivity is found to be 0.59 W/mK [49]. Navarro et al. found the thermal conductivity of $NaNO_3$-MgO CPCMs to be 0.67 W/mK at a similar mass ratio as Na60 E, N.M., [11]. The lower thermal conductivities of vermiculite and perlite CPCMs are expected as their thermal conductivities are quite low. At the same time, in the case of MgO and iron tailings, the conductivity is higher, suggesting that porosity and microstructure morphology play a crucial role in increasing the thermal conductivity of a CPCM.

The correlation between thermal conductivity and microstructure morphology is well-established. In light of this strong link, the XRT images for Samples Na55 and Na60 can offer critical insights into the internal structure that influences the thermal performance of these CPCMs. They visualize the distribution of the various phases within the materials.

The CPCM comprises WFS, X and $NaNO_3$, with densities of 2.51 ± 0.06 g/cm^3, 2.51 g/cm^3, and 2.26 g/cm^3, respectively. The grayscale in the XRT images corresponds to these components, where the lighter gray represents the WFS and sodium bentonite due to their similar densities, and the darker gray indicates the presence of $NaNO_3$ due to its slightly lower density (Fig. 8). The black regions are voids or pores within the CPCM, highlighting areas without material presence.

In Sample Na55, the pores appear uniformly across the cross-sections, confirming that they are integral to the material rather than isolated defects. Notably, the presence of larger, valley-like voids suggests a less uniform structure that may impact the material's overall functionality. Despite this, the gray representing the binder and WFS is evenly distributed, as is the darker gray of the PCM, indicating a good distribution of all components.

Sample Na60's image presents a denser and more consistent microstructure, with a notable absence of the large voids seen in Na55. This finer and more homogeneous distribution indicates a better blending of the materials, which supports the findings of improved thermal conductivity and mechanical strength for Na60 and complements SEM observations. The evenness of the light gray shades across the image suggests an effective encapsulation of the PCM, pointing to a more optimized CPCM structure.

The thermal conductivity of CPCMs is also significantly influenced by the mean pore size and pore size distribution (Fig. 9). This is because the porosity and pore size distribution affect the microstructure of the CPCMs, which in turn affect their ability to transfer heat. Results from X-ray tomography analysis indicate that Na60 samples exhibit a higher mean pore size and a pore size distribution skewed towards larger sizes. On the other hand, Na55 has lower values, despite its higher porosity, implying a microstructure consisting of a larger number of smaller pores. This microstructure has been demonstrated to negatively impact

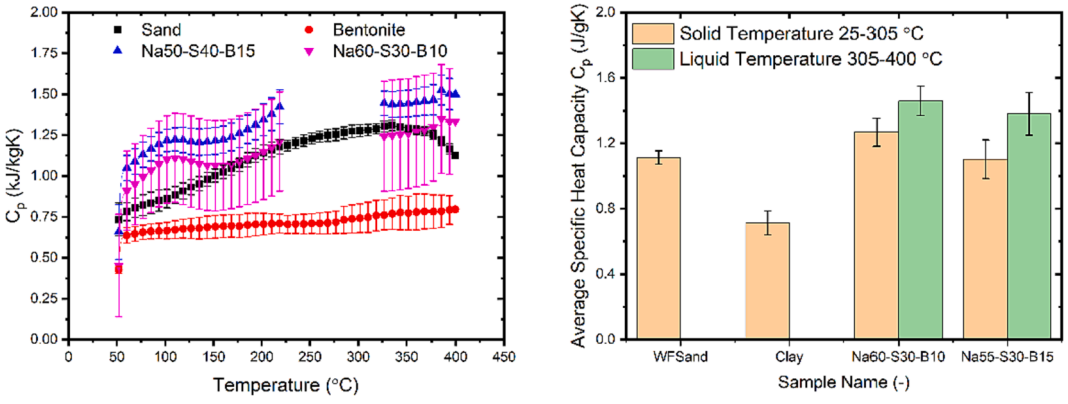

Fig. 6. Specific heat capacity versus temperature (left) and average solid and liquid specific heat capacity (right) of materials investigated in this work.

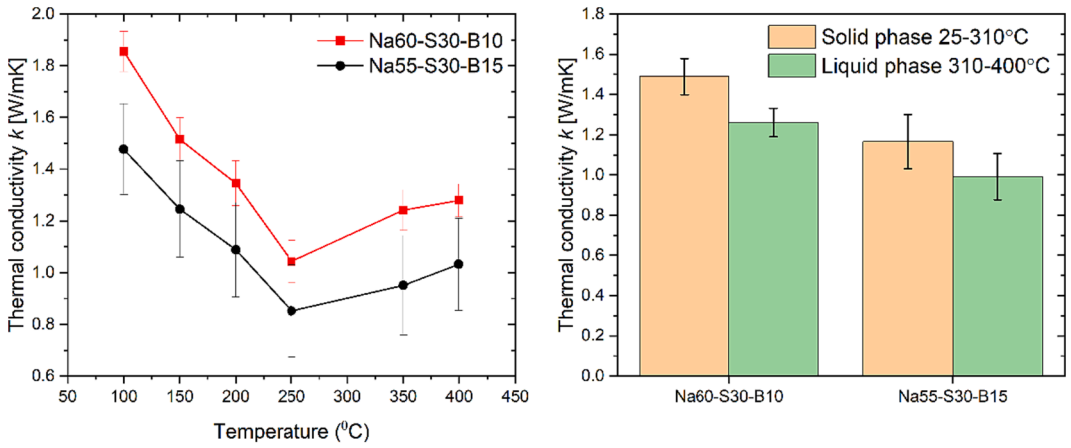

Fig. 7. Thermal conductivity versus temperature (left) and average thermal conductivity in solid and liquid phases (right) of CPCMs investigated in this work.

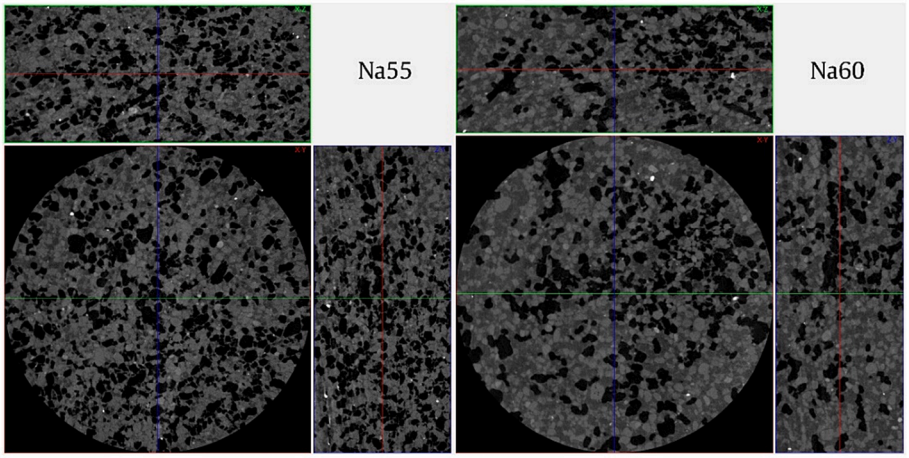

Fig. 8. XRT images displaying cross-sectional views of CPCM samples Na55 (left) and Na60 (right), illustrating the internal structure and distribution of pores within each material.

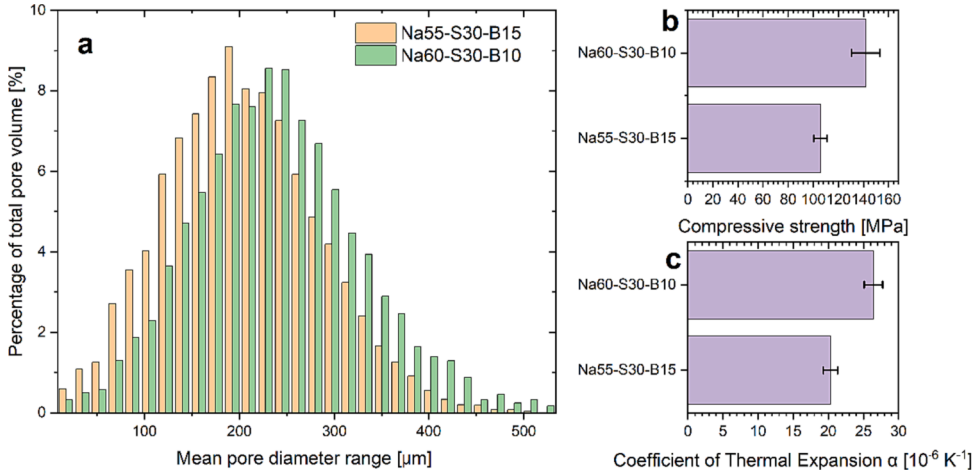

Fig. 9. a: Pore size distribution, b: Compressive strength and c: Coefficient of thermal expansion, of the CPCMs investigated in this work.

thermal conductivity due to the high degree of fragmentation present, which impedes heat transfer and reduces thermal conductivity [20]. This is because smaller pores provide less surface area for heat transfer and cause greater phonon scattering. In contrast, larger pores provide more surface area for heat transfer and allow for better phonon transport [44]. Similar findings have been reported in studies of nickel capillaries and zirconia, where smaller pore sizes were shown to correspond to decreased thermal conductivity for identical levels of porosity [43,52] Therefore, while porosity is an important factor for thermal conductivity in CPCMs, the distribution and size of the pores are also critical for

achieving high thermal conductivity.

Compressive strength is an important mechanical property for phase change materials (PCMs) in thermal energy storage applications. It determines their ability to withstand external mechanical loads without undergoing permanent deformation or failure. This study found that Na60 performs considerably better than Na50 regarding compressive strength (Fig. 6 right).

The compressive strength of porous materials like composite PCMs mainly depends on their porosity [23]. Porosity, in turn, is determined by the volume fraction of voids or pores in the material relative to its total volume. Na60 has 21.3 % lower porosity compared to Na55, which explains its higher compressive strength. This is because a minor decrease in porosity substantially reduces compressive strength due to the exponential relationship between these two properties [32].

In addition to porosity, pore size also plays a critical role in determining the compressive strength of PCMs. A smaller pore size benefits compressive strength, as it indicates a better structure uniformity and load distribution. However, contrary to porosity, the effect of pore size on compressive strength is linear, and in larger pore sizes (>1μm) its effect on compressive strength is minor [29]. It is worth noting that the compressive strength of the fabricated CPCM samples in this study falls within the range of values reported for other PCMs based on phosphogypsum and red mud [5–7]. This highlights the good structural potential of waste foundry sand (WFS) as a viable CPCM matrix alternative.

The coefficient of thermal expansion (CTE) of the two CPCMs, Na50 and Na60, falls within the range reported for moulding sands (~18.6) [10]. This observation is expected as the waste foundry sand (WFS) serves as the matrix material and, therefore, primarily influences the structural behaviour of the CPCMs during thermal processing. However, the CTE values of the CPCMs are slightly larger than the CTE of WFS due to the presence of salt (Fig. 6 right). This is supported by the higher CTE value of Na60, which has a higher PCM content than Na55.

It is worth noting that the CTE of molten $NaNO_3$ is significantly larger than that of WFS by about two orders of magnitude. This disparity results in thermal pressurisation induced by the PCM during heating, especially at molten temperatures. Therefore, the CTE of the CPCM is affected by the thermal behaviour of the PCM and its interaction with the WFS.

Previous studies have shown that there is no clear correlation between the CTE of a material and its porosity [16]. However, considering the two CPCMs with similar compositions, a larger porosity is beneficial as it translates to a higher permeability of the PCM and, in turn, reduces the pressurisation of the matrix [17]. This ultimately results in a decreased CTE. Therefore, a higher porosity can be advantageous in reducing the thermal expansion of the CPCM.

4. Conclusions

Waste foundry sand (WFS) is a by-product of casting industries. After a certain degree of recycling, most sand used in metal casting is disposed of in landfills. Due to increasing landfill taxes, the practice of transporting and maintaining the waste sand accounts for up to 4 % of a typical foundry's turnover. Currently, the USA and China produce over 71 million tonnes of WFS of which only a small fraction is upcycled. This work aims to introduce a novel tangible, and feasible use case of WFS as a TES material. This is realised by combining it with $NaNO_3$ and an additive to form a composite phase change material suitable for medium–high temperature waste heat recovery and TES applications. The main conclusions derived from this study are the following:

- Due to the poor cohesion of WFS, a filler material is required to fabricate a stable CPCM. This is achieved through the use of X.
- CPCMs consisting of mass ratios of 60–30-10 and 55–30-15 of $NaNO_3$ (PCM) – WFS – X are stable after 48 cycles between 25 and 400 °C.
- The energy storage density is 628 ± 27 kJ/kg for Na60 compared to 567 ± 43 kJ/kg for Na55
- The average thermal conductivity of Na60 samples is 24 % higher than Na55 samples (1.38 vs 1.08 W/mK), which is attributed to the higher porosity of Na55 samples.
- The compressive strength of Na60 samples is 141 MPa and 105 MPa for Na55 samples, which is also attributed to the porosity and pore size of the materials.
- The larger porosity is beneficial for the CTE of the CPCMs, due to the lesser forces exerted by the PCM on the matrix material. For this reason, Na60 samples have a higher CTE than Na55 ones (26.4 versus 20.3 10^{-6}·1/K).

Given the above, this work demonstrates a stable CPCM based on WFS, with good thermal performance. Hopefully, this work can serve as the onset for a novel utilisation pathway for WFS, a practice that can considerably promote energy efficiency and sustainability in the context of industrial symbiosis.

Declaration of competing interest

The authors declare that they have no known competing financial interests or personal relationships that could have appeared to influence the work reported in this paper.

Acknowledgements

The authors would like to acknowledge Transforming Foundation Industries Network + in the context of THERMCAST (EPSRC grant EP/V026402/1) as well as the European Commision under Grant agreement ID: 101068507.

References

[1] M.Y. Abdelsalam, H.M. Teamah, M.F. Lightstone, J.S. Cotton, Hybrid thermal energy storage with phase change materials for solar domestic hot water applications: direct versus indirect heat exchange systems, Renew. Energy 147 (2020), https://doi.org/10.1016/j.renene.2019.08.121.
[2] R. Agathokleous, G. Bianchi, G. Panayiotou, L. Aresti, M.C. Argyrou, G.S. Georgiou, S.A. Tassou, H. Jouhara, S.A. Kalogirou, G.A. Florides, P. Christodoulides, Waste heat recovery in the EU industry and proposed new technologies, Energy Procedia 161 (2019) 489–496, https://doi.org/10.1016/j.egypro.2019.02.064.
[3] H. Ait Ousaleh, S. Sair, S. Mansouri, Y. Abboud, M. Zahouily, A. Faik, A.E. Bouari, Enhanced inorganic salts stability using bentonite clay for high-performance and low-cost thermochemical energy storage, J. Energy Storage 49 (2022), https://doi.org/10.1016/j.est.2022.104140.
[4] A. Anagnostopoulos, A. Alexiadis, Y. Ding, Molecular dynamics simulation of solar salt (NaNO3-KNO3) mixtures, Sol. Energy Mater. Sol. Cells 200 (2019), 109897, https://doi.org/10.1016/j.solmat.2019.04.019.
[5] A. Anagnostopoulos, M. Navarro, A. Ahmad, Y. Ding, G. Gaidajis, Valorization of phosphogypsum as a thermal energy storage material for low temperature applications, J. Clean. Prod. 342 (2022), 130839, https://doi.org/10.1016/J.JCLEPRO.2022.130839.
[6] A. Anagnostopoulos, M.E. Navarro, M. Stefanidou, Y. Ding, G. Gaidajis, Red mud-molten salt composites for medium-high temperature thermal energy storage and waste heat recovery applications, J. Hazard. Mater. 413 (2021), https://doi.org/10.1016/j.jhazmat.2021.125407.
[7] A. Anagnostopoulos, M.E. Navarro, M. Stefanidou, P. Seferlis, G. Gaidajis, Y. Ding, Effect of carbon on the performance of red mud-molten salt composites for thermal management and waste heat recovery applications, J. Energy Storage 44 (2021), 103363, https://doi.org/10.1016/j.est.2021.103363.
[8] A. Anagnostopoulos, A. Palacios, M.H. Navarro, S. Fereres, Y. Ding, Effect of SiO2 nanoparticle addition on the wetting and rheological properties of solar salt, Sol. Energy Mater. Sol. Cells 210 (2020), 110483, https://doi.org/10.1016/j.solmat.2020.110483.
[9] B. Bhardwaj, P. Kumar, Waste foundry sand in concrete: a review, Constr. Build. Mater. (2017), https://doi.org/10.1016/j.conbuildmat.2017.09.010.
[10] A. Bobrowski, D. Drożyński, J. Jakubski, M. Szumera, K. Kaczmarska, B. Grabowska, Thermal deformation of moulding and core sands with an inorganic binder containing a relaxation additive, Arch. Foundry Eng. 18 (2018), https://doi.org/10.24425/afe.2018.125175.
[11] E, n.m.,, Thermal properties of a novel medium temperature thermal energy storage composite based on sodium nitrate as phase change material, 12th Int. Conf. Heat Transf. Fluid Mech. Thermodyn. (2016).
[12] O. Ellabban, H. Abu-Rub, F. Blaabjerg, 2014. Renewable energy resources: current status, future prospects and their enabling technology. Renew. Sustain. Energy Rev. https://doi.org/10.1016/j.rser.2014.07.113.
[13] European Commission, 2016. 2030 Energy Strategy [WWW Document]. Europa.

[14] A.I. Fernández, C. Barreneche, L. Miró, S. Brückner, L.F. Cabeza, A.I. Fernández et al., 2021. Waste heat recovery using thermal energy storage, in: Advances in Thermal Energy Storage Systems. https://doi.org/10.1016/b978-0-12-819885-8.00022-x.
[15] Z. Ge, F. Ye, H. Cao, G. Leng, Y. Qin, Y. Ding, Carbonate-salt-based composite materials for medium- and high-temperature thermal energy storage, Particuology 15 (2014) 77–81, https://doi.org/10.1016/j.partic.2013.09.002.
[16] S. Ghabezloo, Micromechanical analysis of the effect of porosity on the thermal expansion coefficient of heterogeneous porous materials, Int. J. Rock Mech. Min. Sci. 55 (2012), https://doi.org/10.1016/j.ijrmms.2012.07.001.
[17] S. Ghabezloo, 2010. Effect of porosity on the thermal expansion coefficient: a discussion of the paper "Effects of mineral admixtures on the thermal expansion properties of hardened cement paste" by Z.H. Shui, R. Zhang, W. Chen, D. Xuan, Constr. Build. Mater. 24 (9) (2010) 1761-1767. Constr. Build. Mater. https://doi.org/10.1016/j.conbuildmat.2010.03.006.
[18] Y. Guney, Y.D. Sari, M. Yalcin, A. Tuncan, S. Donmez, Re-usage of waste foundry sand in high-strength concrete, Waste Manag. 30 (2010) 1705–1713, https://doi.org/10.1016/J.WASMAN.2010.02.018.
[19] Q. Guo, T. Wang, Study on preparation and thermal properties of sodium nitrate/silica composite as shape-stabilized phase change material, Thermochim. Acta. (2015), https://doi.org/10.1016/j.tca.2015.05.023.
[20] X. Huai, W. Wang, Z. Li, Analysis of the effective thermal conductivity of fractal porous media, Appl. Therm. Eng. 27 (2007) 2815–2821, https://doi.org/10.1016/J.APPLTHERMALENG.2007.01.031.
[21] IEA, Global Energy Review: CO2 Emissions in 2020, Glob, Energy Rev, 2021.
[22] F. Jiang, L. Zhang, X. She, C. Li, D. Cang, X. Liu, Y. Xuan, Y. Ding, Skeleton materials for shape-stabilization of high temperature salts based phase change materials: a critical review, Renew. Sustain. Energy Rev. 119 (2020), 109539, https://doi.org/10.1016/j.rser.2019.109539.
[23] L. Jiang, Y. Guan, Pore structure and its effect on strength of high-volume fly ash paste, Cem. Concr. Res. 29 (1999), https://doi.org/10.1016/S0008-8846(99)00034-4.
[24] H. Jouhara, N. Khordehgah, S. Almahmoud, B. Delpech, A. Chauhan, S.A. Tassou, Waste heat recovery technologies and applications, Therm. Sci. Eng. Prog. 6 (2018) 268–289, https://doi.org/10.1016/j.tsep.2018.04.017.
[25] H. Jouhara, A. Żabnieńska-Góra, N. Khordehgah, D. Ahmad, T. Lipinski, Latent thermal energy storage technologies and applications: a review, Int. J. Thermofluids 5–6 (2020), https://doi.org/10.1016/j.ijft.2020.100039.
[26] G. Kaur, R. Siddique, A. Rajor, Influence of fungus on properties of concrete made with waste foundry sand, J. Mater. Civ. Eng. 25 (2013), https://doi.org/10.1061/(asce)mt.1943-5533.0000521.
[27] A.I. Khalaf, M.A. Hegazy, D.E. El-Nashar, Synthesis and characterization of cationic gemini surfactant modified Na–bentonite and its applications for rubber nanocomposites, Polym. Compos. 38 (2017) 396–403, https://doi.org/10.1002/PC.23598.
[28] J.M. Khatib, B.A. Herki, S. Kenai, Capillarity of concrete incorporating waste foundry sand, Constr. Build. Mater. 47 (2013), https://doi.org/10.1016/j.conbuildmat.2013.05.013.
[29] D. Li, Z. Li, C. Lv, G. Zhang, Y. Yin, A predictive model of the effective tensile and compressive strengths of concrete considering porosity and pore size, Constr. Build. Mater. 170 (2018), https://doi.org/10.1016/j.conbuildmat.2018.03.028.
[30] R. Li, J. Zhu, W. Zhou, X. Cheng, Y. Li, Thermal properties of sodium nitrate-expanded vermiculite form-stable composite phase change materials, Mater. Des. 104 (2016), https://doi.org/10.1016/j.matdes.2016.05.039.
[31] R. Li, J. Zhu, W. Zhou, X. Cheng, Y. Li, Thermal compatibility of sodium nitrate/expanded perlite composite phase change materials, Appl. Therm. Eng. (2016), https://doi.org/10.1016/j.applthermaleng.2016.03.108.
[32] D.M. Liu, Influence of porosity and pore size on the compressive strength of porous hydroxyapatite ceramic, Ceram. Int. 23 (1997), https://doi.org/10.1016/S0272-8842(96)00009-0.
[33] M. Liu, Q. Jin, P. Shen, Cold sintering of NaNO3/MgO heat-storage composite, Ceram. Int. 46 (2020) 28955–28960, https://doi.org/10.1016/j.ceramint.2020.08.066.
[34] A. Lomonacoa, D. Haillot, E. Pernot, E. Franquet, J.P. Bédécrats, Thermal characterization of sodium nitrate - Sodium nitrite compounds for thermal storage applications. In: ECOS 2015–28th International Conference on Efficiency, Cost, Optimization, Simulation and Environmental Impact of Energy Systems, 2015.
[35] J. Malinauskaite, H. Jouhara, L. Ahmad, M. Milani, L. Montorsi, M. Venturelli, Energy efficiency in industry: EU and national policies in Italy and the UK, Energy 172 (2019), https://doi.org/10.1016/j.energy.2019.01.130.
[36] M. Mavroulidou, D. Lawrence, Can waste foundry sand fully replace structural concrete sand? J. Mater. Cycles Waste Manag. 21 (2019) 594–605, https://doi.org/10.1007/S10163-018-00821-1/FIGURES/8.
[37] L. Miró, J. Gasia, L.F. Cabeza, Thermal energy storage (TES) for industrial waste heat (IWH) recovery: a review, Appl. Energy. (2016), https://doi.org/10.1016/j.apenergy.2016.06.147.
[38] R.-A. Mitran, D. Lincu, L. Buhălţeanu, D. Berger, C. Matei, Shape-stabilized phase change materials using molten NaNO3 – KNO3 eutectic and mesoporous silica matrices, Sol. Energy Mater. Sol. Cells 215 (2020), 110644, https://doi.org/10.1016/j.solmat.2020.110644.
[39] M.J. O'Neill, Measurement of specific heat functions by differential scanning calorimetry, Anal. Chem. 38 (1966), https://doi.org/10.1021/ac60242a011.
[40] F.A. Olutoge, S.O.A. Olawale, M.A. Gbadamosi, Strength behavior of concrete produced with foundry sand as fine aggregate replacement, Int. J. Emerg. Technol. Adv, Eng, 2015, p. 5.
[41] A. Palacios, C. Barreneche, M.E. Navarro, Y. Ding, Thermal energy storage technologies for concentrated solar power – a review from a materials perspective, Renew. Energy. (2019), https://doi.org/10.1016/j.renene.2019.10.127.
[42] B. Peris, J. Navarro-Esbrí, F. Molés, A. Mota-Babiloni, Experimental study of an ORC (organic Rankine cycle) for low grade waste heat recovery in a ceramic industry, Energy (2015), https://doi.org/10.1016/j.energy.2015.03.065.
[43] G. Pia, L. Casnedi, U. Sanna, Porosity and pore size distribution influence on thermal conductivity of yttria-stabilized zirconia: experimental findings and model predictions, Ceram. Int. 42 (2016), https://doi.org/10.1016/j.ceramint.2015.12.122.
[44] G. Pia, U. Sanna, An intermingled fractal units model to evaluate pore size distribution influence on thermal conductivity values in porous materials, Appl. Therm. Eng. 65 (2014), https://doi.org/10.1016/j.applthermaleng.2014.01.037.
[45] M.R. Sabour, G. Derhamjani, M. Akbari, A.M. Hatami, Global trends and status in waste foundry sand management research during the years 1971–2020: a systematic analysis, Environ. Sci. Pollut. Res. 28 (2021) 37312–37321, https://doi.org/10.1007/S11356-021-13251-8/FIGURES/7.
[46] F. Santiago, A.E. Mucientes, M. Osorio, C. Rivera, Preparation of composites and nanocomposites based on bentonite and poly(sodium acrylate). effect of amount of bentonite on the swelling behaviour, Eur. Polym. J. 43 (2007) 1–9, https://doi.org/10.1016/J.EURPOLYMJ.2006.07.023.
[47] R. Siddique, A. Noumowe, Utilization of spent foundry sand in controlled low-strength materials and concrete, Resour. Conserv. Recycl. (2008), https://doi.org/10.1016/j.resconrec.2008.09.007.
[48] R. Siddique, G. Singh, Utilization of waste foundry sand (WFS) in concrete manufacturing, Resour. Conserv. Recycl. (2011), https://doi.org/10.1016/j.resconrec.2011.05.001.
[49] Z. Su, Y. Tu, X. Chen, Y. Zhang, B. Han, C. Anderson, T. Jiang, A value-added multistage utilization process for the gradient-recovery tin, iron and preparing composite phase change materials (C-PCMs) from tailings, Sci. Rep. 9 (2019), https://doi.org/10.1038/s41598-019-50536-y.
[50] B. Xu, Z. Li, Paraffin/diatomite composite phase change material incorporated cement-based composite for thermal energy storage, Appl. Energy 105 (2013), https://doi.org/10.1016/j.apenergy.2013.01.005.
[51] G. Xu, G. Leng, C. Yang, Y. Qin, Y. Wu, H. Chen, L. Cong, Y. Ding, Sodium nitrate – diatomite composite materials for thermal energy storage, Sol. Energy 146 (2017) 494–502, https://doi.org/10.1016/j.solener.2017.03.003.
[52] J. Xu, Y. Zou, M. Fan, L. Cheng, Effect of pore parameters on thermal conductivity of sintered LHP wicks, Int. J. Heat Mass Transf. 55 (2012), https://doi.org/10.1016/j.ijheatmasstransfer.2012.01.028.
[53] H. Yang, W. Zhang, Y. Zhu, Y. Shao, Y. Shao, X. Zhang, Preparation and characterisation of sodium nitrate/stone-sawing mud shape-stabilized phase change materials for medium-high temperature thermal energy storage, J. Energy Storage 56 (2022), 106047, https://doi.org/10.1016/J.EST.2022.106047.